

ULRR

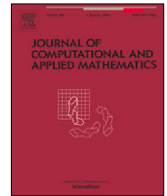
Fast computation of the Lorentz force induced by longitudinal electromagnetic stirring

Item Type	Article
Authors	Vynnycky, Michael;Nick, A.S.;Assunção, Milton
Citation	Journal of Computational and Applied Mathematics 416, 114565
Publisher	Elsevier
Download date	2026-06-08 02:42:16
Item License	https://creativecommons.org/licenses/by-nc-sa/4.0/
Link to Item	https://doi.org/10.34961/researchrepository-ul.21673472



Contents lists available at ScienceDirect

Journal of Computational and Applied Mathematics

journal homepage: www.elsevier.com/locate/cam

Fast computation of the Lorentz force induced by longitudinal electromagnetic stirring

M. Vynnycky^{a,b,*}, A.S. Nick^{b,1}, M. Assunção^{c,2}^a Mathematics Applications Consortium for Science and Industry (MACSI), Department of Mathematics and Statistics, University of Limerick, Limerick, V94 T9PX, Ireland^b Division of Processes, Department of Materials Science and Engineering, KTH Royal Institute of Technology, Brinellvägen 23, 100 44 Stockholm, Sweden^c Institute of Computing, Federal University of Mato Grosso, Cuiabá, Mato Grosso 78060-900, Brazil

ARTICLE INFO

Article history:

Received 30 June 2021

Received in revised form 15 February 2022

Keywords:

Electromagnetic stirring

Maxwell equations

Continuous casting

ABSTRACT

In this work, we revisit a recent transient three-dimensional (3D) model for longitudinal electromagnetic stirring in the continuous casting of rectangular steel blooms. Whereas the earlier work was able to demonstrate accurate approximations to the solutions in two asymptotic limits, both of which gave economical alternatives to time-consuming 3D computations, here we show that the original governing equations can be manipulated to a form that allows for rapid computation even outside of these asymptotic limits. The resulting formulation requires the numerical solution of two steady-state complex Helmholtz-like equations in two dimensions that are coupled via a non-standard internal interface condition that is reminiscent of that occurring in the study of Marangoni convection; these equations are then solved numerically using the finite-element software Comsol Multiphysics. With this formulation, it is possible to compute the time-averaged Lorentz force components in a way that requires around four orders of magnitude less computational time than the fully 3D approach.

© 2022 The Author(s). Published by Elsevier B.V. This is an open access article under the CC BY license (<http://creativecommons.org/licenses/by/4.0/>).

1. Introduction

Electromagnetic stirring (EMS) is a technique that has long been used in the continuous casting of steel as a way to affect the flow of molten metal, and thereby the solidification structure, with a view to increasing yield and productivity [1]. One particular example, and the main focus of this work, is that of longitudinal EMS; a schematic for this is shown in Fig. 1, which depicts a stirrer operating in the continuous casting of rectangular steel blooms. Here, a travelling wave is passed in the direction of casting, x , by means of a linear induction motor, and this generates a Lorentz force that in turn results in a fluid flow. In parallel with technical developments, mathematical modelling has often been used in order to provide a more quantitative understanding of what effect EMS actually has and how its use can be optimized, not just for rectangular blooms, but also for round blooms, square billets and slabs [2].

* Corresponding author at: Mathematics Applications Consortium for Science and Industry (MACSI), Department of Mathematics and Statistics, University of Limerick, Limerick, V94 T9PX, Ireland.

E-mail address: michael.vynnycky@ul.ie (M. Vynnycky).

¹ Present address: LKAB, 981 86 Kiruna, Sweden.

² Present address: Mathematics Applications Consortium for Science and Industry (MACSI), Department of Mathematics and Statistics, University of Limerick, Limerick, V94 T9PX, Ireland.

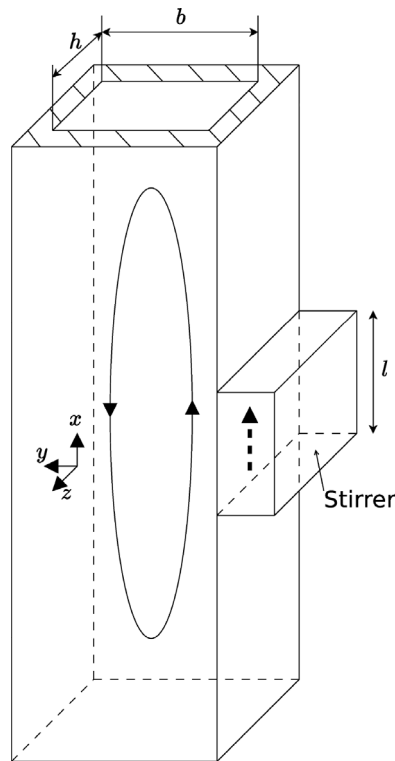


Fig. 1. Schematic for the longitudinal stirring of blooms. A travelling wave is passed parallel to the casting (x) direction.

Mathematically, the models in question for longitudinal EMS involve the simultaneous solution of the time-dependent Navier–Stokes equations for the velocity field of the molten metal and the time-dependent Maxwell equations for the induced magnetic flux density [3–5]. However, the fact that the magnetic Reynolds number is small allows the equations to be decoupled, so that the Maxwell equations can be solved first; thence, the Lorentz force can be computed and inserted as a source term into the Navier–Stokes equations. Moreover, a further simplification that is often employed makes use of the fact that the magnetic field frequency is large enough to allow the input of the time-averaged Lorentz force into the Navier–Stokes equations.

In spite of these simplifications, the computation of the time-dependent Maxwell equations in three dimensions (3D) alone is still time-consuming [6,7], even with currently available techniques. As an alternative, Nick and Vynnycky [6] and Nick et al. [7] used asymptotic methods to obtain reliable approximate solutions for the problem of longitudinal EMS in two different limits. Identifying the product of the wave vector of the electromagnetic field and the bloom width as a key dimensionless parameter, denoted by Δ , they obtained asymptotic solutions for $\Delta \ll 1$ and $\Delta \gg 1$. Quantitative comparison with the solutions to the time-dependent 3D Maxwell equations indicated good agreement for $\Delta \leq 0.01$ and $\Delta \geq 10$; nevertheless, it was shown in [7] that there was no agreement when $\Delta = 0.1$, implying that, for $10^{-2} \leq \Delta \leq 10$, the only option available is to perform very time-consuming 3D computations in order to determine magnetic flux density, the current density and the Lorentz force components. Thus, the purpose of this manuscript is to consider, still in the low magnetic Reynolds number limit as in [6,7], a mathematical formulation that will circumvent the use of 3D computations and yield the quantities required in a timely manner for all values of Δ .

The layout of the paper is as follows. In Section 2, we recap the mathematical formulation of the problem, whereas in Section 3, we nondimensionalize the governing equations. The new analysis, in terms of the dimensionless parameter Δ , is given in Section 4, whilst Section 5 details the numerical method used to solve the resulting model equations: this consists of just two two-dimensional (2D) time-independent complex partial differential equations, albeit with awkward discontinuity conditions at interior interfaces. The results are presented in Section 6, and the conclusions follow in Section 7.

2. Model formulation

2.1. Governing equations

As already depicted in Fig. 1, we consider a linear travelling stirrer that is located at

$$y = 0, -h/2 \leq z \leq h/2, -l \leq x \leq 0,$$

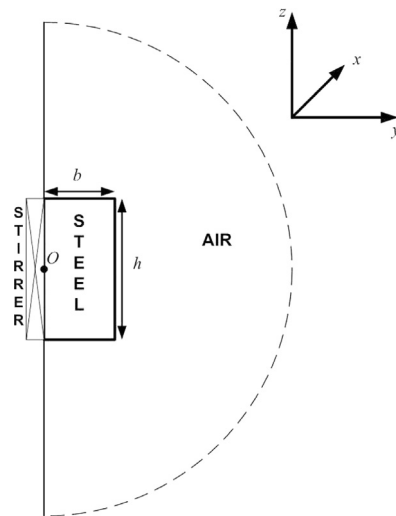


Fig. 2. Cross-section in the $y - z$ plane of Fig. 1, showing the stirrer, steel and air. O denotes the origin of the coordinates.

and delivers a pulse that is proportional to $\cos(\omega t - \lambda x)$, where t is time, ω is the angular frequency of the electric current and λ is the wave vector of the electromagnetic field, which is given by $\lambda = \pi/p$, with p as the distance between the north and south poles in the inductor; this profile makes it appropriate to assume a sinusoidal steady state condition. Furthermore, the stirrer operates on a molten steel region whose cross-section occupies $0 \leq y \leq b, -h/2 \leq z \leq h/2$, as illustrated in Fig. 2; thus, the steel region is surrounded by air on the other three sides. As explained previously in [6,7], although this is a drastic simplification of the situation in an actual continuous caster, it is nevertheless sufficient for carrying out a meaningful analysis as regards determining the three-dimensional and transient characteristics of the magnetic flux density and the Lorentz force.

In considering the solution of Maxwell's equations in the magnetohydrodynamic (MHD) approximation, we have the following:

- the magnetic field constraint, given by

$$\nabla \cdot \mathbf{B} = 0, \tag{1}$$

where \mathbf{B} is the magnetic flux density vector;

- Ampère's law, expressed through

$$\mu \mathbf{J} = \nabla \times \mathbf{B}, \tag{2}$$

where μ is the magnetic permeability, which is taken to be constant in both air and steel, and \mathbf{J} is the electrical current density vector;

- Faraday's law, which is written as

$$\nabla \times \mathbf{E} = -\frac{\partial \mathbf{B}}{\partial t}, \tag{3}$$

where \mathbf{E} is the electric field;

- Ohm's law,

$$\mathbf{J} = \sigma (\mathbf{E} + \mathbf{v} \times \mathbf{B}), \tag{4}$$

where \mathbf{v} is the velocity vector, which will simply be taken to be zero, in line with the assumption of low magnetic Reynolds number, and σ is the electrical conductivity of the medium in question, which is taken to be constant in both air and steel.

It is then straightforward to manipulate Eqs. (2)-(4) to obtain

$$\sigma \mu \frac{\partial \mathbf{B}}{\partial t} = \nabla^2 \mathbf{B}, \tag{5}$$

which still has to be solved in tandem with Eq. (1). Thus, with $\mathbf{B} = (B_x, B_y, B_z)$, we have, on writing out Eqs. (1) and (5) in full,

$$\frac{\partial B_x}{\partial x} + \frac{\partial B_y}{\partial y} + \frac{\partial B_z}{\partial z} = 0, \tag{6}$$

$$\sigma \mu \frac{\partial B_x}{\partial t} = \frac{\partial^2 B_x}{\partial x^2} + \frac{\partial^2 B_x}{\partial y^2} + \frac{\partial^2 B_x}{\partial z^2}, \tag{7}$$

$$\sigma \mu \frac{\partial B_y}{\partial t} = \frac{\partial^2 B_y}{\partial x^2} + \frac{\partial^2 B_y}{\partial y^2} + \frac{\partial^2 B_y}{\partial z^2}, \tag{8}$$

$$\sigma \mu \frac{\partial B_z}{\partial t} = \frac{\partial^2 B_z}{\partial x^2} + \frac{\partial^2 B_z}{\partial y^2} + \frac{\partial^2 B_z}{\partial z^2}. \tag{9}$$

Once the components of \mathbf{B} have been determined, the principal quantities of interest are the components of the Lorentz force, F_x , F_y and F_z , which are given by

$$F_x = J_y B_z - J_z B_y, \quad F_y = J_z B_x - J_x B_z, \quad F_z = J_x B_y - J_y B_x, \tag{10}$$

where $\mathbf{J} = (J_x, J_y, J_z)$, with

$$\begin{pmatrix} J_x \\ J_y \\ J_z \end{pmatrix} = \frac{1}{\mu} \begin{pmatrix} \frac{\partial B_z}{\partial y} - \frac{\partial B_y}{\partial z} \\ \frac{\partial B_x}{\partial z} - \frac{\partial B_z}{\partial x} \\ \frac{\partial B_y}{\partial x} - \frac{\partial B_x}{\partial y} \end{pmatrix}. \tag{11}$$

Finally, F_x , F_y and F_z can be used to calculate the time-averaged Lorentz force components - \bar{F}_x , \bar{F}_y and \bar{F}_z - via

$$\bar{F}_k = \frac{1}{2\pi/\omega} \int_0^{2\pi/\omega} F_k dt', \quad k = x, y, z; \tag{12}$$

the integrals in Eq. (12) are taken with respect to time over one period of oscillation, $2\pi/\omega$.

2.2. Boundary conditions

At $y = 0$, as discussed in our earlier work [6–8], a well-posed problem is obtained if we prescribe the tangential components of \mathbf{B} ; thus, following the notation in [6,7], we write

$$B_x = \begin{cases} \alpha(z) \cos(\omega t - \lambda x) & \text{for } |z| \leq h/2 \\ 0 & \text{for } |z| > h/2 \end{cases}, \tag{13}$$

$$B_z = \begin{cases} \beta(z) \cos(\omega t - \lambda x) & \text{for } |z| \leq h/2 \\ 0 & \text{for } |z| > h/2 \end{cases}. \tag{14}$$

In [6,7], no particular constraints were placed on $\alpha(z)$ and $\beta(z)$, and a number of different choices were ultimately made for the purposes of quantitatively illustrating the model results: in [6],

$$\alpha(z) = B_0, \quad \beta(z) = 0, \tag{15}$$

and

$$\alpha(z) = B_0 \left(\frac{z}{b}\right)^2, \quad \beta(z) = B_0 \left(\frac{z}{b}\right)^2; \tag{16}$$

in [7],

$$\alpha(z) = B_0, \quad \beta(z) = 0, \tag{17}$$

$$\alpha(z) = 0, \quad \beta(z) = B_0, \tag{18}$$

and

$$\alpha(z) = B_0, \quad \beta(z) = B_0. \tag{19}$$

Consequently, in four of these cases—(15),(16),(17) and (19) - B_x is discontinuous at $|z| = h/2$, whereas B_z is discontinuous at $|z| = h/2$ in three of them—(16),(18) and (19). Here, however, as we shall see later, it will be necessary to pay particular attention to these potential discontinuities.

In the air far from the steel, it is natural to expect that the magnetic flux density will be vanishingly small; thus, we take

$$\mathbf{B} \rightarrow 0 \quad \text{as } x, z \rightarrow \pm\infty, y \rightarrow +\infty. \tag{20}$$

2.3. Interfacial conditions

At the steel–air interfaces at $y = b$, $|z| \leq h/2$ and $|z| = h/2$, $0 \leq y \leq b$, we have the usual electromagnetic interface conditions between two media [9, p. 8]. These are: the continuity of the tangential components of the magnetic field strength; the continuity of the normal component of the magnetic flux density; and the continuity of the tangential components of the electric field. These are written, respectively, as

$$\left[\frac{\mathbf{B} \cdot \mathbf{t}}{\mu} \right]_{-}^{+} = 0, \tag{21}$$

$$[\mathbf{B} \cdot \mathbf{n}]_{-}^{+} = 0, \tag{22}$$

$$[\mathbf{E} \cdot \mathbf{t}]_{-}^{+} = 0, \tag{23}$$

where \mathbf{n} and \mathbf{t} are, respectively, the unit normal and tangential vectors at these interfaces. In equations ((21)–(23)), $[]_{-}^{+}$ denotes the difference in the value of a function in the air (+) and in the steel (–). In full, and rewriting in terms of the components of \mathbf{B} alone, Eqs. (21)–(23) are: at $y = b$, $|z| \leq h/2$,

$$\left[\frac{B_x}{\mu} \right]_{-}^{+} = 0, \tag{24}$$

$$[B_y]_{-}^{+} = 0, \tag{25}$$

$$\left[\frac{B_z}{\mu} \right]_{-}^{+} = 0, \tag{26}$$

$$\left[\frac{1}{\sigma \mu} \left(\frac{\partial B_z}{\partial y} - \frac{\partial B_y}{\partial z} \right) \right]_{-}^{+} = 0, \tag{27}$$

$$\left[\frac{1}{\sigma \mu} \left(\frac{\partial B_x}{\partial y} - \frac{\partial B_y}{\partial x} \right) \right]_{-}^{+} = 0; \tag{28}$$

at $|z| = h/2$, $0 \leq y \leq b$,

$$\left[\frac{B_x}{\mu} \right]_{-}^{+} = 0, \tag{29}$$

$$\left[\frac{B_y}{\mu} \right]_{-}^{+} = 0, \tag{30}$$

$$[B_z]_{-}^{+} = 0, \tag{31}$$

$$\left[\frac{1}{\sigma \mu} \left(\frac{\partial B_z}{\partial y} - \frac{\partial B_y}{\partial z} \right) \right]_{-}^{+} = 0, \tag{32}$$

$$\left[\frac{1}{\sigma \mu} \left(\frac{\partial B_x}{\partial z} - \frac{\partial B_z}{\partial x} \right) \right]_{-}^{+} = 0. \tag{33}$$

We can note here in passing that, although it is the steel region that is of primary interest, there is nothing in the interface conditions to suggest that the air region can be simply neglected; for this reason, it is necessary to formulate the problem for both air and steel regions.

2.4. Initial conditions

Strictly speaking, Eqs. (6)–(9) require initial conditions. However, as we will be seeking periodic solutions, since the problem is driven by the time-periodic boundary conditions in (13) and (14), it suffices simply to set

$$\mathbf{B} = \mathbf{0}, \tag{34}$$

with the expectation that the effect of the initial transient should disappear after a couple of periods of oscillation [6,7].

2.5. Model parameters

Representative model parameters are given in Table 1; note that these were the values used in [6,7], as well as much earlier in [5]. Observe, in particular, that the value given for μ_s is the same as that for air. In fact, this marks the lower limit for austenitic stainless steels, which have a relative permeability in the range 1–7 [10]; on the other hand, the relative permeability of ferritic, martensitic and duplex stainless steels can be as high as 10^3 . However, this fact does not affect the applicability of the model equations given here.

Table 1
Model parameters.

Parameter	Symbol	Value
Steel width	b	0.25 m
Characteristic magnetic flux density	B_0	0.02 T
Current frequency	f	50 Hz
Steel breadth	h	0.35 m
Stirrer length	l	1.2 m
Air magnetic permeability	μ_a	$1.2566 \times 10^{-6} \text{ V s A}^{-1}\text{m}^{-1}$
Steel magnetic permeability	μ_s	$1.2566 \times 10^{-6} \text{ V s A}^{-1}\text{m}^{-1}$
Air electrical conductivity	σ_a	$3 \times 10^{-15} \text{--} 8 \times 10^{-15} \text{ A V}^{-1}\text{m}^{-1}$
Steel electrical conductivity	σ_s	$7.14 \times 10^5 \text{ A V}^{-1}\text{m}^{-1}$

3. Nondimensionalization

The equations of Section 2 are nondimensionalized by setting

$$X = \frac{x}{l}, \quad Y = \frac{y}{b}, \quad Z = \frac{z}{b}, \quad \tau = \frac{\omega t}{2\pi}, \tag{35}$$

and, for $k = x, y, z$ and $K = X, Y, Z$,

$$B_K = \frac{B_k}{B_0}, \quad E_K = \frac{E_k}{B_0/\sigma_s\mu_s b}, \quad J_K = \frac{J_k}{B_0/\mu_s b}, \quad F_K = \frac{F_k}{B_0^2/\mu_s b},$$

where B_0 is a characteristic value for the magnetic flux density, and σ_s and μ_s are, respectively, the electrical conductivity and the magnetic permeability of the steel. Eqs. (6)–(9) give

$$\varepsilon \frac{\partial B_X}{\partial X} + \frac{\partial B_Y}{\partial Y} + \frac{\partial B_Z}{\partial Z} = 0, \tag{36}$$

$$\Omega \frac{\partial B_X}{\partial \tau} = \varepsilon^2 \frac{\partial^2 B_X}{\partial X^2} + \frac{\partial^2 B_X}{\partial Y^2} + \frac{\partial^2 B_X}{\partial Z^2}, \tag{37}$$

$$\Omega \frac{\partial B_Y}{\partial \tau} = \varepsilon^2 \frac{\partial^2 B_Y}{\partial X^2} + \frac{\partial^2 B_Y}{\partial Y^2} + \frac{\partial^2 B_Y}{\partial Z^2}, \tag{38}$$

$$\Omega \frac{\partial B_Z}{\partial \tau} = \varepsilon^2 \frac{\partial^2 B_Z}{\partial X^2} + \frac{\partial^2 B_Z}{\partial Y^2} + \frac{\partial^2 B_Z}{\partial Z^2}, \tag{39}$$

where $\varepsilon = b/l$ and $\Omega = f\sigma\mu b^2$; however, note that the values for Ω for air and steel, which we will denote by Ω_a and Ω_s respectively, are different. Also, from Eqs. (11), (10) and (12), respectively, we have

$$\begin{pmatrix} J_X \\ J_Y \\ J_Z \end{pmatrix} = \begin{pmatrix} \frac{\partial B_Z}{\partial Y} - \frac{\partial B_Y}{\partial Z} \\ \frac{\partial B_X}{\partial Z} - \varepsilon \frac{\partial B_Z}{\partial X} \\ \varepsilon \frac{\partial B_Y}{\partial X} - \frac{\partial B_X}{\partial Y} \end{pmatrix}, \tag{40}$$

$$\begin{pmatrix} F_X \\ F_Y \\ F_Z \end{pmatrix} = \begin{pmatrix} J_Y B_Z - J_Z B_Y \\ J_Z B_X - J_X B_Z \\ J_X B_Y - J_Y B_X \end{pmatrix}, \tag{41}$$

$$\bar{F}_K = \int_0^1 F_K dt', \quad K = X, Y, Z. \tag{42}$$

The boundary conditions (13)–(20) are then: at $Y = 0$,

$$B_X = \begin{cases} \bar{\alpha}(Z) \cos(2\pi\tau - \Lambda X) & \text{for } |Z| \leq H/2 \\ 0 & \text{for } |Z| > H/2 \end{cases}, \tag{43}$$

$$B_Z = \begin{cases} \bar{\beta}(Z) \cos(2\pi\tau - \Lambda X) & \text{for } |Z| \leq H/2 \\ 0 & \text{for } |Z| > H/2 \end{cases}, \tag{44}$$

where

$$\bar{\alpha} = \frac{\alpha}{[\alpha]}, \quad \bar{\beta} = \frac{\beta}{[\beta]}, \quad \Lambda = \lambda l, \quad H = \frac{h}{b}, \tag{45}$$

with $[\alpha]$ and $[\beta]$ denoting, respectively, the scales for α and β ; as $X, Z \rightarrow \pm\infty, Y \rightarrow +\infty$,

$$B_X, B_Y, B_Z \rightarrow 0. \tag{46}$$

The interfacial conditions, (24)–(33), become: at $Y = 1, |Z| \leq H/2$,

$$\left[\frac{B_X}{\mu} \right]_{-}^{+} = 0, \tag{47}$$

$$[B_Y]_{-}^{+} = 0, \tag{48}$$

$$\left[\frac{B_Z}{\mu} \right]_{-}^{+} = 0, \tag{49}$$

$$\left[\frac{1}{\sigma \mu} \left(\frac{\partial B_Z}{\partial Y} - \frac{\partial B_Y}{\partial Z} \right) \right]_{-}^{+} = 0, \tag{50}$$

$$\left[\frac{1}{\sigma \mu} \left(\frac{\partial B_X}{\partial Y} - \frac{\partial B_Y}{\partial X} \right) \right]_{-}^{+} = 0; \tag{51}$$

at $|Z| = H/2, 0 \leq Y \leq 1$,

$$\left[\frac{B_X}{\mu} \right]_{-}^{+} = 0, \tag{52}$$

$$\left[\frac{B_Y}{\mu} \right]_{-}^{+} = 0, \tag{53}$$

$$[B_Z]_{-}^{+} = 0, \tag{54}$$

$$\left[\frac{1}{\sigma \mu} \left(\frac{\partial B_Z}{\partial Y} - \frac{\partial B_Y}{\partial Z} \right) \right]_{-}^{+} = 0, \tag{55}$$

$$\left[\frac{1}{\sigma \mu} \left(\frac{\partial B_X}{\partial Z} - \frac{\partial B_Z}{\partial X} \right) \right]_{-}^{+} = 0. \tag{56}$$

The initial condition (34) is now

$$B_X, B_Y, B_Z = 0 \quad \text{at } \tau = 0. \tag{57}$$

4. Analysis

As in [6,7], Eq. (36) and the boundary conditions in (43) will imply that, for B_X, B_Y and B_Z , we should try solutions of the form

$$B_X, B_Y, B_Z \sim \cos(2\pi\tau - \lambda X), \sin(2\pi\tau - \lambda X).$$

To this end, we begin by setting

$$\left. \begin{aligned} B_k &= \Re \left(\mathcal{B}_k(Y, Z) e^{i(2\pi\tau - \lambda X)} \right), \\ E_k &= \Re \left(\mathcal{E}_k(Y, Z) e^{i(2\pi\tau - \lambda X)} \right), \end{aligned} \right\} \quad k = X, Y, Z, \tag{58}$$

where \Re denotes the real part of a complex number and $i = \sqrt{-1}$. Eqs. (36)–(39) become, for $i = a, s$,

$$-\Delta i \mathcal{B}_X + \frac{\partial \mathcal{B}_Y}{\partial Y} + \frac{\partial \mathcal{B}_Z}{\partial Z} = 0, \tag{59}$$

$$(2\pi \Omega i + \Delta^2) \mathcal{B}_X = \frac{\partial^2 \mathcal{B}_X}{\partial Y^2} + \frac{\partial^2 \mathcal{B}_X}{\partial Z^2}, \tag{60}$$

$$(2\pi \Omega i + \Delta^2) \mathcal{B}_Y = \frac{\partial^2 \mathcal{B}_Y}{\partial Y^2} + \frac{\partial^2 \mathcal{B}_Y}{\partial Z^2}, \tag{61}$$

$$(2\pi \Omega i + \Delta^2) \mathcal{B}_Z = \frac{\partial^2 \mathcal{B}_Z}{\partial Y^2} + \frac{\partial^2 \mathcal{B}_Z}{\partial Z^2}, \tag{62}$$

where $\Delta = \lambda b$. In terms of $\mathcal{B}_X, \mathcal{B}_Y$ and \mathcal{B}_Z , the boundary conditions are now: at $Y = 0$,

$$\mathcal{B}_X = \begin{cases} \bar{\alpha}(Z) & \text{for } |Z| \leq H/2 \\ 0 & \text{for } |Z| > H/2 \end{cases}, \tag{63}$$

$$\mathcal{B}_Z = \begin{cases} \bar{\beta}(Z) & \text{for } |Z| \leq H/2 \\ 0 & \text{for } |Z| > H/2 \end{cases}; \tag{64}$$

as $Y \rightarrow +\infty, Z \rightarrow \pm\infty$,

$$\mathcal{B}_X, \mathcal{B}_Y, \mathcal{B}_Z \rightarrow 0. \tag{65}$$

As for the interfacial conditions, these are: at $Y = 1, |Z| \leq H/2,$

$$\left[\frac{\mathcal{B}_X}{\mu} \right]_-^+ = 0, \tag{66}$$

$$[\mathcal{B}_Y]_-^+ = 0, \tag{67}$$

$$\left[\frac{\mathcal{B}_Z}{\mu} \right]_-^+ = 0, \tag{68}$$

$$\left[\frac{1}{\sigma\mu} \left(\frac{\partial \mathcal{B}_Z}{\partial Y} - \frac{\partial \mathcal{B}_Y}{\partial Z} \right) \right]_-^+ = 0, \tag{69}$$

$$\left[\frac{1}{\sigma\mu} \left(i\Delta \mathcal{B}_Y + \frac{\partial \mathcal{B}_X}{\partial Y} \right) \right]_-^+ = 0; \tag{70}$$

at $|Z| = H/2, 0 \leq Y \leq 1,$

$$\left[\frac{\mathcal{B}_X}{\mu} \right]_-^+ = 0, \tag{71}$$

$$\left[\frac{\mathcal{B}_Y}{\mu} \right]_-^+ = 0, \tag{72}$$

$$[\mathcal{B}_Z]_-^+ = 0, \tag{73}$$

$$\left[\frac{1}{\sigma\mu} \left(\frac{\partial \mathcal{B}_Z}{\partial Y} - \frac{\partial \mathcal{B}_Y}{\partial Z} \right) \right]_-^+ = 0, \tag{74}$$

$$\left[\frac{1}{\sigma\mu} \left(i\Delta \mathcal{B}_Z + \frac{\partial \mathcal{B}_X}{\partial Z} \right) \right]_-^+ = 0. \tag{75}$$

In view of the ansatz suggested by Eq. (58), which leads to a time-independent problem for $\mathcal{B}_X, \mathcal{B}_Y$ and $\mathcal{B}_Z,$ there is now no need to consider (57).

4.1. \mathcal{B}_Y

Consider first $Y = 0.$ The idea here will be to combine Eqs. (59), (63) and (64), in order to obtain a boundary condition for $\mathcal{B}_Y.$ We have

$$\frac{\partial \mathcal{B}_Y}{\partial Y} = \mathcal{F}(Z) + \begin{cases} i\Delta \bar{\alpha}(Z) - \bar{\beta}'(Z) & \text{for } |Z| \leq H/2 \\ 0 & \text{for } |Z| > H/2 \end{cases}, \tag{76}$$

with

$$\mathcal{F}(Z) = \bar{\beta} \left(-\frac{H}{2} \right) \delta \left(Z + \frac{H}{2} \right) - \bar{\beta} \left(\frac{H}{2} \right) \delta \left(Z - \frac{H}{2} \right), \tag{77}$$

where the prime denotes differentiation with respect to Z and δ denotes the Dirac delta function; consequently, the use of δ in (76) takes into account the possibility of the appearance of the two point sources in $\partial \mathcal{B}_Z / \partial Z$ which arise as a result of the two Heaviside jumps in \mathcal{B}_Z suggested by Eq. (44).

Now consider $Y = 1, |Z| \leq H/2.$ Eqs. (59) and (66) imply

$$\left[\frac{1}{\mu} \left(\frac{\partial \mathcal{B}_Y}{\partial Y} + \frac{\partial \mathcal{B}_Z}{\partial Z} \right) \right]_-^+ = 0, \tag{78}$$

whence Eq. (68) implies

$$\left[\frac{1}{\mu} \frac{\partial \mathcal{B}_Y}{\partial Y} \right]_-^+ = 0; \tag{79}$$

together with Eq. (67), this gives a complete set of conditions for \mathcal{B}_Y at this interface.

Consider now $|Z| = H/2, 0 \leq Y \leq 1.$ If we are able to find an interface condition for \mathcal{B}_Y that supplements (72), we would have a well-posed problem for $\mathcal{B}_Y,$ thereby decoupling it from \mathcal{B}_X and $\mathcal{B}_Z;$ however, this turns out not to be possible, and \mathcal{B}_Y is coupled to \mathcal{B}_Z via Eq. (74).

4.2. \mathcal{B}_Z

The situation is similar for \mathcal{B}_Z . Consider $|Z| = H/2, 0 \leq Y \leq 1$. Eqs. (59) and (71) imply

$$\left[\frac{1}{\mu} \left(\frac{\partial \mathcal{B}_Y}{\partial Y} + \frac{\partial \mathcal{B}_Z}{\partial Z} \right) \right]_{-}^{+} = 0, \tag{80}$$

whence Eq. (72) implies

$$\left[\frac{1}{\mu} \frac{\partial \mathcal{B}_Z}{\partial Z} \right]_{-}^{+} = 0; \tag{81}$$

together with Eq. (73), this gives a complete set of interface conditions for \mathcal{B}_Z .

On the other hand, for $Y = 1, |Z| \leq H/2$, we will have Eqs. (68) and (69), with \mathcal{B}_Z coupled to \mathcal{B}_Y via the latter.

4.3. \mathcal{B}_X

At this point, we may notice that the boundary conditions given in Sections 4.1 and 4.2 constitute the full set required to solve Eqs. (61) and (62) for \mathcal{B}_Y and \mathcal{B}_Z ; consequently, the problem for \mathcal{B}_Y and \mathcal{B}_Z has decoupled from that for \mathcal{B}_X . However, there now appear to be two routes to determine \mathcal{B}_X : either simply to use Eq. (59) directly, so that

$$\mathcal{B}_X = -\frac{i}{\Delta} \left(\frac{\partial \mathcal{B}_Y}{\partial Y} + \frac{\partial \mathcal{B}_Z}{\partial Z} \right), \tag{82}$$

or to solve Eq. (60), subject to (63),(65),(66),(70),(71) and (75). Of course, the two approaches should give identical results, although this is perhaps not entirely obvious at this point: it is clear that \mathcal{B}_X , as given by Eq. (82), will satisfy (60),(63),(65),(66) and (71), but not (70) and (75). However, to demonstrate that Eq. (70) is indeed satisfied, we note that, on using Eq. (59), Eq. (70) becomes

$$\left[\frac{i}{\sigma \mu \Delta} \left(-\Delta^2 \mathcal{B}_Y + \frac{\partial}{\partial Y} \left(\frac{\partial \mathcal{B}_Y}{\partial Y} + \frac{\partial \mathcal{B}_Z}{\partial Z} \right) \right) \right]_{-}^{+} = 0,$$

which, on using Eq. (61), gives

$$\frac{i}{\Delta} \left[\left(2\pi i \mathcal{B}_Y + \frac{1}{\sigma \mu} \frac{\partial}{\partial Z} \left(\frac{\partial \mathcal{B}_Z}{\partial Y} - \frac{\partial \mathcal{B}_Y}{\partial Z} \right) \right) \right]_{-}^{+} = 0,$$

which is evidently the case, in view of Eqs. (67) and (69). The corresponding result for Eq. (75) can be found in a similar way, employing Eqs. (59),(61),(72) and (74).

4.4. Summary

At this stage, we are left solving, for $i = a, s$,

$$(2\pi \Omega_i + \Delta^2) \mathcal{B}_Y = \frac{\partial^2 \mathcal{B}_Y}{\partial Y^2} + \frac{\partial^2 \mathcal{B}_Y}{\partial Z^2}, \tag{83}$$

$$(2\pi \Omega_i + \Delta^2) \mathcal{B}_Z = \frac{\partial^2 \mathcal{B}_Z}{\partial Y^2} + \frac{\partial^2 \mathcal{B}_Z}{\partial Z^2}, \tag{84}$$

subject to: at $Y = 0$,

$$\frac{\partial \mathcal{B}_Y}{\partial Y} = \mathcal{F}(Z) + \begin{cases} i\Delta \bar{\alpha}(Z) - \bar{\beta}'(Z) & \text{for } |Z| \leq H/2 \\ 0 & \text{for } |Z| > H/2 \end{cases}, \tag{85}$$

$$\mathcal{B}_Z = \begin{cases} \bar{\beta}(Z) & \text{for } |Z| \leq H/2 \\ 0 & \text{for } |Z| > H/2 \end{cases}; \tag{86}$$

as $Y \rightarrow +\infty, Z \rightarrow \pm\infty$,

$$\mathcal{B}_Y, \mathcal{B}_Z \rightarrow 0; \tag{87}$$

at $Y = 1, |Z| \leq H/2$,

$$\left[\frac{1}{\mu} \frac{\partial \mathcal{B}_Y}{\partial Y} \right]_{-}^{+} = 0, \tag{88}$$

$$[\mathcal{B}_Y]_{-}^{+} = 0, \tag{89}$$

$$\left[\frac{\mathcal{B}_Z}{\mu} \right]_{-}^{+} = 0, \tag{90}$$

$$\left[\frac{1}{\sigma\mu} \left(\frac{\partial \mathcal{B}_Z}{\partial Y} - \frac{\partial \mathcal{B}_Y}{\partial Z} \right) \right]_{-}^{+} = 0; \tag{91}$$

at $|Z| = H/2, 0 \leq Y \leq 1,$

$$\left[\frac{1}{\mu} \frac{\partial \mathcal{B}_Z}{\partial Z} \right]_{-}^{+} = 0, \tag{92}$$

$$\left[\frac{\mathcal{B}_Y}{\mu} \right]_{-}^{+} = 0, \tag{93}$$

$$[\mathcal{B}_Z]_{-}^{+} = 0, \tag{94}$$

$$\left[\frac{1}{\sigma\mu} \left(\frac{\partial \mathcal{B}_Z}{\partial Y} - \frac{\partial \mathcal{B}_Y}{\partial Z} \right) \right]_{-}^{+} = 0. \tag{95}$$

Mathematically, we can note that (83) and (84) are Helmholtz-like equations, albeit complex because of the pre-multiplication factors on the left-hand sides. Also, interface conditions (91) and (95) resemble that which occurs in the study of Marangoni convection, wherein the shear stress at the interface of two fluids is related to the tangential temperature or concentration gradient and the interface is approximated to be planar [11,12]; more exactly, in Eq. (91), \mathcal{B}_Z is analogous to the tangential velocity component and \mathcal{B}_Y is analogous to the temperature or concentration, whereas in Eq. (95), the roles are reversed. Computationally, we see that the numerical task is non-standard, in that, although \mathcal{B}_Y and $\frac{1}{\mu} \frac{\partial \mathcal{B}_Y}{\partial Y}$ are continuous at $Y = 1$ for $|Z| \leq H/2$, \mathcal{B}_Y and $\frac{1}{\mu} \frac{\partial \mathcal{B}_Y}{\partial Z}$ will not be continuous at $|Z| = H/2$ for $0 \leq Y \leq 1$; moreover, the discontinuity involves $\frac{\partial \mathcal{B}_Z}{\partial Y}$. Note also that \mathcal{B}_Z and $\frac{1}{\mu} \frac{\partial \mathcal{B}_Z}{\partial Z}$ will be continuous at this boundary, but \mathcal{B}_Z and $\frac{1}{\mu} \frac{\partial \mathcal{B}_Z}{\partial Y}$ will not be continuous at $Y = 1$ for $|Z| \leq H/2$. In addition, there are two singularities in $\frac{\partial \mathcal{B}_Y}{\partial Y}$ at $Y = 0, Z = \pm H/2$ if $\bar{\beta}(\pm H/2) \neq 0$, and it would be numerically advantageous to reformulate the problem, so as to remove them; in principle, this can be done and is explained further in the Appendix. However, the case $\bar{\beta}(\pm H/2) \neq 0$ implies that \mathcal{B}_Z would be discontinuous at $Z = \pm H/2$, which would be unphysical; indeed, this case was only introduced, somewhat artificially, in [6] as a way to generate a benchmark solution for comparison against an asymptotic solution. Here, instead, we consider just the case when $\bar{\beta}(\pm H/2) = 0$, so that the situation is more physically motivated; moreover, we may use some of the 3D solutions that were generated numerically in [7] to compare our new method against, rather than having to perform new time-consuming computations which those 3D solutions entailed. Hence, for the remainder of this paper, we consider $\bar{\alpha} \equiv 1, \bar{\beta} \equiv 0$, corresponding to $\alpha = B_0, \beta = 0$, respectively; this means that we take $[\alpha] = [\beta] = B_0$ in Eq. (45).

5. Numerical solution

To solve Eqs. (83)–(87), the finite-element software Comsol Multiphysics was used. Because of the nature of the steel-air interface conditions, which imply that $\mathcal{B}_Y, \mathcal{B}_Z$ and their normal derivatives are not continuous at all interfaces, it was necessary to use four PDE General Form modules: two each for \mathcal{B}_Y and \mathcal{B}_Z . Thus, the modules are for four variables, which we denote by $\mathcal{B}_Y^{(1)}, \mathcal{B}_Y^{(2)}, \mathcal{B}_Z^{(1)}$ and $\mathcal{B}_Z^{(2)}$. Referring to Fig. 2, the geometry needs to be divided in the manner shown in the subplots in Fig. 3, i.e. with the air domain being cut by two arbitrary curves, most easily taken to be straight lines, from the steel corners out to computational infinity; these are denoted by C_* . In addition, the plots in Fig. 3 show which variable is solved for in which domain. The construct is such that:

- $\mathcal{B}_Y^{(1)}$ and $\mu^{-1} \partial \mathcal{B}_Y^{(1)} / \partial Y$ will be continuous at $Y = 1, |Z| \leq H/2$;
- $\mathcal{B}_Z^{(1)}$ and $\mu^{-1} \partial \mathcal{B}_Z^{(1)} / \partial Z$ will be continuous at $|Z| = H/2, 0 \leq Y \leq 1$;
- at the curves C_* ,

$$\begin{aligned} \mathcal{B}_Y^{(1)} &= \mathcal{B}_Y^{(2)}, & \mathbf{n}_* \cdot \nabla \mathcal{B}_Y^{(1)} &= \mathbf{n}_* \cdot \nabla \mathcal{B}_Y^{(2)}, \\ \mathcal{B}_Z^{(1)} &= \mathcal{B}_Z^{(2)}, & \mathbf{n}_* \cdot \nabla \mathcal{B}_Z^{(1)} &= \mathbf{n}_* \cdot \nabla \mathcal{B}_Z^{(2)}, \end{aligned}$$

where \mathbf{n}_* denotes the unit vector normal to C_* .

Moreover, four Weak Form, Boundary modules are also required, in order to take account of the tangential derivatives of \mathcal{B}_Y at $Y = 1$ and \mathcal{B}_Z at $|Z| = H/2$ in Eqs. (91) and (95), respectively; thus, two of these Weak Form, Boundary modules are required at $Y = 1$ and two at $|Z| = H/2$, one on each side of each boundary. The computational domain was taken as

$$Y^2 + Z^2 \leq R_\infty^2, \quad Y \geq 0,$$

with $R_\infty = 4$; thus, R_∞ is four times greater than the width of the steel region. The domain was discretized using second-order Lagrangian triangular elements, giving the mesh shown in Fig. 4; as evident from this figure, substantial refinement

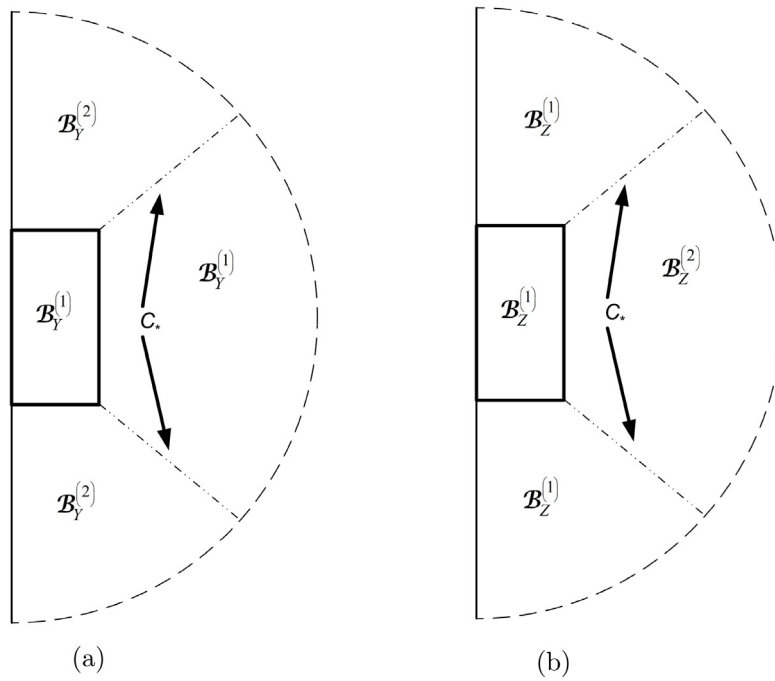


Fig. 3. Domain decomposition for the PDEs for: (a) B_Y ; (b) B_Z .

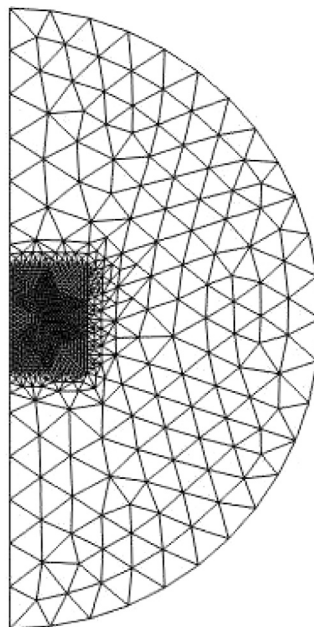


Fig. 4. Mesh used for 2D computations.

was used for the steel region and, overall, the mesh had a total of around 1800 elements, corresponding to around 7900 degrees of freedom, which we denote by N_{dof} . For the computations, Comsol's steady-state solver was employed; the convergence criterion used to obtain solutions was

$$\left(\frac{1}{N_{\text{dof}}} \sum_{N=1}^{N_{\text{dof}}} |E_N|^2 \right)^{1/2} < R_{\text{tol}}, \tag{96}$$

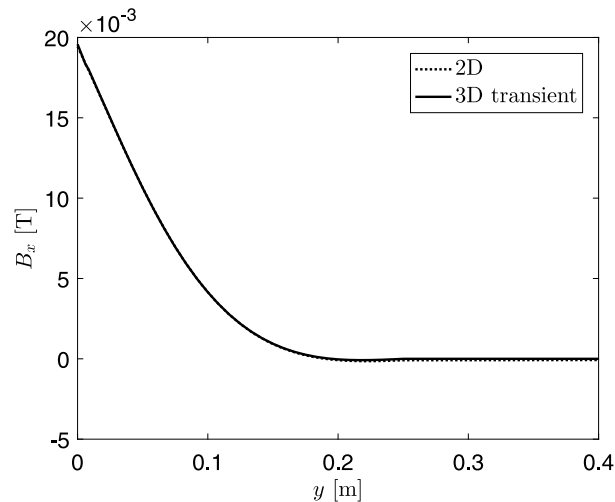


Fig. 5. The x -component of magnetic flux density vector, B_x , vs. distance from the stirrer, y , for $z = 0.0$ m, $t = 0.06$ s, $x = -0.6$ m, for $\Delta = 0.1$, as obtained from full 3D computations in [7] and the method in this paper for $\bar{\alpha} = 1$, $\bar{\beta} = 0$.

where R_{tol} is the relative tolerance, set equal to 10^{-10} , and E_N is the estimated error in the latest approximation to the N^{th} component of the true solution vector for the N^{th} degree of freedom. These 2D computations were carried out on an architecture similar to that used for the 3D model, i.e. an Intel(R) Core(TM) i7-8700 CPU @ 3.20GHz×6 processor with a 32 GB RAM. The typical run time for the 2D computations was of the order of one second, whereas those for 3D computations was of the order of three hours; this was incorrectly stated in [7] as being 9–11 h, which was actually the time taken to compute for three different values of Δ , but even taking into account the correction, the new method requires around four orders of magnitude less computation time.

6. Results

To demonstrate that the new 2D steady-state method is able to produce the same solutions as the original 3D transient method, we consider the case when $\Delta = 0.1$: in Fig. 7(a) in [7], there was already a considerable difference between the result obtained from 3D numerical simulations and the asymptotic solution for small Δ .

Although the development in Sections 4 and 5 was in dimensionless variables, we present the results in dimensional variables, as that is how the results in [7] were given. First of all, Figs. 5 and 6 compare the respective profiles for B_x and B_y at $z = 0$ m, $t = 0.06$ s, $x = -0.6$ m as computed in [7] and using the method of this paper; note that $x = -0.6$ m corresponds to the midpoint of the stirrer in the x -direction. As is evident, the agreement is very good.

Figs. 7 and 8 compare the respective profiles for F_x and F_y at $z = 0$ m, $t = 0.06$ s, $x = -0.6$ m as computed in [7] and using the method of this paper; here also, it is evident that there is good agreement.

Next, Figs. 9 and 10 show comparisons for \bar{F}_x and \bar{F}_y , respectively; these are obtained in compact form by noting that

$$(\bar{F}_x, \bar{F}_y, \bar{F}_z) = \frac{B_0^2}{2\mu_s b} (\Re(\mathcal{J}) \times \Re(\mathcal{B}) + \Im(\mathcal{J}) \times \Im(\mathcal{B})), \tag{97}$$

where

$$\mathcal{J} = \nabla \times \mathcal{B}, \tag{98}$$

with $\mathcal{B} = (B_x, B_y, B_z)$, and once again we see that the agreement is very good, with the curves literally on top of each other in both cases.

Lastly, we note that we have not given any comparisons for B_z , F_z and \bar{F}_z ; in fact, this was also not done for the case of $\alpha = B_0$ and $\beta = 0$ in [6] for $\Delta \gg 1$ and [7] for $\Delta \ll 1$. In particular, when $\alpha = B_0$ and $\beta = 0$, $B_z \equiv 0$ for $\Delta \gg 1$ [6], and $B_z \sim O(\Delta)$ for $\Delta \ll 1$ [7]; in general, $B_z \ll B_x, B_y$ and it is difficult to obtain a meaningful comparison in this case, as the computational tolerance would have to be set to a prohibitively low value. It was for this reason that Nick and Vynnycky [6] introduced the profiles given by Eq. (16), to ensure that B_x, B_y and B_z are all of the same order of magnitude; even then, they made comparisons not at $z = 0$, where $\alpha = 0, \beta = 0$, which would again lead to difficulties as regards comparison since B_x and B_z are both zero there due to symmetry about $z = 0$, but at $z = h/4$. However, with hindsight, we can see that Eq. (16) would be of limited use in making comparisons between the earlier 3D solutions and

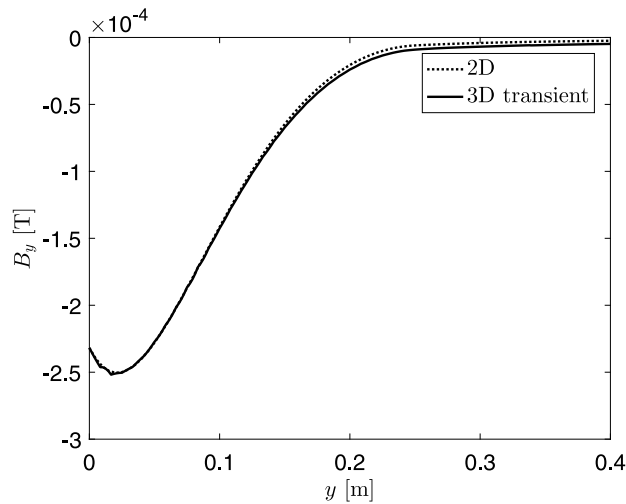


Fig. 6. The y-component of magnetic flux density vector, B_y , vs. distance from the stirrer, y , for $z = 0.0$ m, $t = 0.06$ s, $x = -0.6$ m, for $\Delta = 0.1$, as obtained from full 3D computations in [7] and the method in this paper for $\bar{\alpha} = 1$, $\bar{\beta} = 0$.

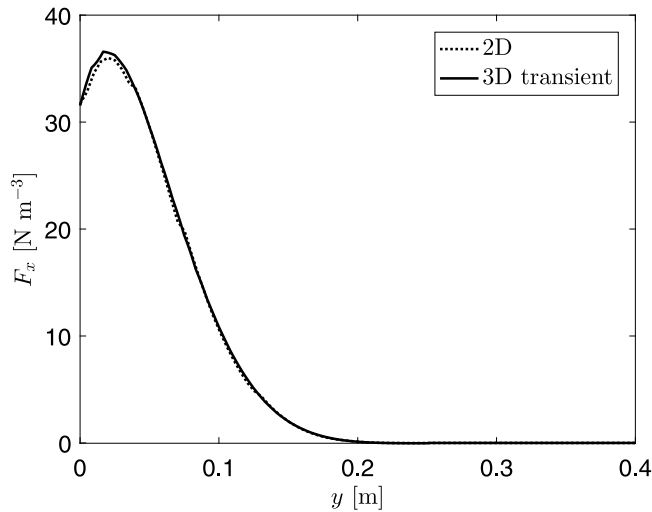


Fig. 7. The x-component of the Lorentz force density vector, \bar{F}_x , vs. distance from the stirrer, y , for $z = 0.0$ m, $t = 0.06$ s, $x = -0.6$ m, for $\Delta = 0.1$, as obtained from full 3D computations in [7] and the method in this paper for $\bar{\alpha} = 1$, $\bar{\beta} = 0$.

our new 2D method, albeit for a different reason: the profile for $\beta(z)$ would lead to the previously discussed singularities at $y = 0$, $z = \pm h/2$. Without doubt, in this context, a wiser choice would have been, e.g.

$$\beta(z) = B_0 \left\{ 1 - \left(\frac{2z}{h} \right)^2 \right\};$$

however, this would have needed the computation of further 3D solutions, which was not our focus here.

7. Conclusions

In this work, we have revisited a recent transient 3D model for longitudinal electromagnetic stirring in the continuous casting of rectangular steel blooms [6,7]. Whereas these earlier works were able to demonstrate accurate approximations to the solutions in two asymptotic limits, both of which gave economical alternatives to time-consuming 3D computations, here we have shown that the original governing equations can be manipulated to a form that allows for rapid computation even outside of these asymptotic limits. The resulting formulation requires the numerical solution of two 2D steady-state complex Helmholtz-like equations that are coupled via non-standard internal interface conditions that are reminiscent

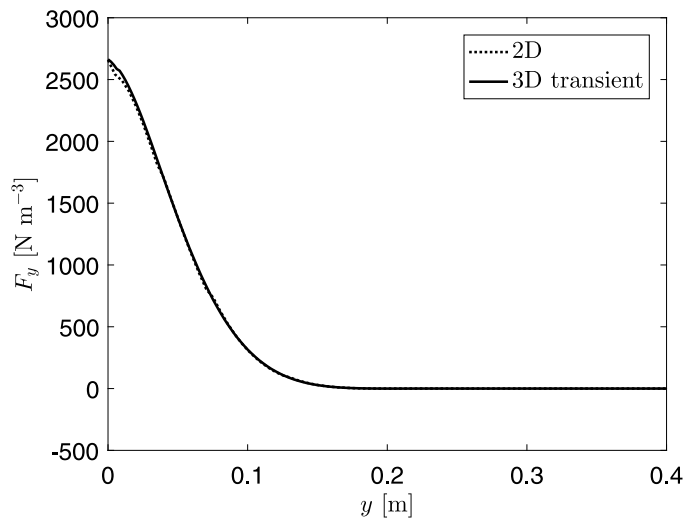


Fig. 8. The y-component of the Lorentz force density vector, \bar{F}_y , vs. distance from the stirrer, y , for $z = 0.0$ m, $t = 0.06$ s, $x = -0.6$ m, for $\Delta = 0.1$, as obtained from full 3D computations in [7] and the method in this paper for $\bar{\alpha} = 1, \bar{\beta} = 0$.

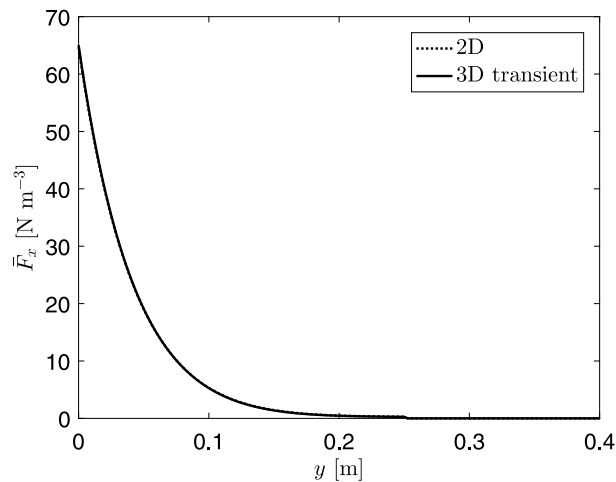


Fig. 9. The time average of the x-component of the Lorentz force density vector, \bar{F}_x , vs. distance from the stirrer, y , for $z = 0.0$ m, $x = -0.6$ m, for $\Delta = 0.1$, as obtained from full 3D computations in [7] and the method in this paper for $\bar{\alpha} = 1, \bar{\beta} = 0$.

of that occurring in the study of Marangoni convection; these equations were then solved numerically using the finite-element software Comsol Multiphysics. With this formulation, it was possible to compute the time-averaged Lorentz force components in a way that required around four orders of magnitude less computational time than the fully 3D approach.

It is now worth considering how these results can be extended further. Although the analysis was carried out for a stirrer operating at one frequency, it can form the basis for studying modulated EMS [13–15], wherein magnetic fields of different frequencies are applied simultaneously, with the intention that the resulting Lorentz force has a constant time-averaged component and a time-varying component; this is believed to achieve more vigorous stirring than is possible when using just one frequency. In this case, Eqs. (13) and (14) would be replaced by

$$B_x = \begin{cases} \sum_{i=1}^n \alpha_i(z) \cos(\omega_i t - \lambda_i x) & \text{for } |z| \leq h/2 \\ 0 & \text{for } |z| > h/2 \end{cases}, \tag{99}$$

$$B_z = \begin{cases} \sum_{i=1}^n \beta_i(z) \cos(\omega_i t - \lambda_i x) & \text{for } |z| \leq h/2 \\ 0 & \text{for } |z| > h/2 \end{cases}, \tag{100}$$

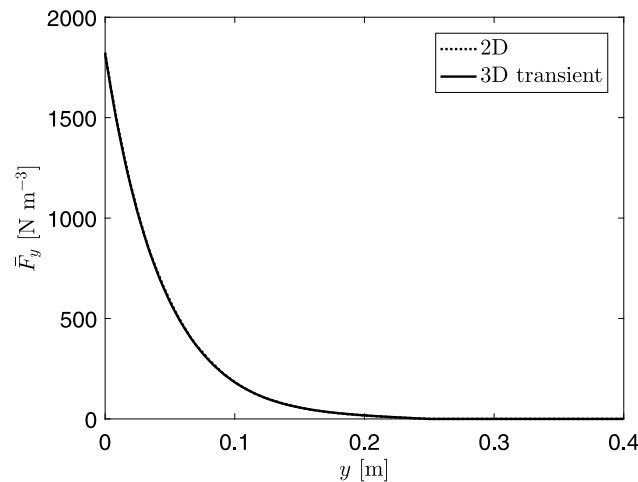


Fig. 10. The time average of the y -component of the Lorentz force density vector, \bar{F}_y , vs. distance from the stirrer, y , for $z = 0.0$ m, $x = -0.6$ m, for $\Delta = 0.1$, as obtained from full 3D computations in [7] and the method in this paper for $\bar{\alpha} = 1, \bar{\beta} = 0$.

assuming n different angular frequencies $(\omega_i)_{i=1,\dots,n}$ and maintaining generality by introducing $(\alpha_i(z), \beta_i(z), \lambda_i)_{i=1,\dots,n}$ also. We can now simply set

$$\mathbf{B} = \sum_{i=1}^n \mathbf{B}_i,$$

which will lead to n independent problems of the type considered in this paper. Since each of these can now be computed very quickly using our new method, so can the components of the Lorentz force.

Lastly, we can contemplate whether the ideas developed in this paper may be used for other applications. Whilst we are unaware of any other industrial situations where a linear travelling stirrer is used in this way, we believe that our methodology could also be used in horizontal stirring in the continuous casting of slabs [2,4,16,17]; recall that this paper was specifically dedicated to the longitudinal stirring in the continuous casting of blooms. In the case of slabs, and with reference to Fig. 1, it is the case that $h \gg b$, and a wave is passed in the z -direction instead; thus, Eqs. (13) and (14) would be replaced by

$$B_x = \begin{cases} \alpha(x) \cos(\omega t - \lambda z) & \text{for } |z| \leq h/2 \\ 0 & \text{for } |z| > h/2 \end{cases}, \tag{101}$$

$$B_z = \begin{cases} \beta(x) \cos(\omega t - \lambda z) & \text{for } |z| \leq h/2 \\ 0 & \text{for } |z| > h/2 \end{cases}, \tag{102}$$

respectively. It is then reasonable to expect that Eq. (58) would be replaced by

$$\left. \begin{aligned} B_k &= \Re\{\mathcal{B}_k(X, Y) e^{i(2\pi\tau - \lambda Z)}\}, \\ E_k &= \Re\{\mathcal{E}_k(X, Y) e^{i(2\pi\tau - \lambda Z)}\}, \end{aligned} \right\} \quad k = X, Y, Z, \tag{103}$$

resulting in a two-dimensional problem, with X and Y as the independent variables.

Appendix. Removal of singularities when $\bar{\beta}(\pm H/2) \neq 0$

In this case, it is clear from Eq. (85) that $\frac{\partial \mathcal{B}_Y}{\partial Y}$ has Dirac delta-function singularities at $Z = \pm H/2$. We now define

$$\tilde{\mathcal{B}}_Y := \mathcal{B}_Y - \beta_- \left(1 - \frac{\theta_-}{\pi}\right) + \beta_+ \left(1 - \frac{\theta_+}{\pi}\right),$$

where $\beta_- = \bar{\beta}(-H/2)$, $\beta_+ = \bar{\beta}(H/2)$, and θ_- and θ_+ are defined as shown in Fig. A.1, in other words,

$$\theta_- = \begin{cases} \tan^{-1}\left(\frac{-Y}{Z+H/2}\right) & Z < -H/2 \\ \pi + \tan^{-1}\left(\frac{-Y}{Z+H/2}\right) & Z > -H/2 \end{cases},$$

$$\theta_+ = \begin{cases} \tan^{-1}\left(\frac{-Y}{Z-H/2}\right) & Z < -H/2 \\ \pi + \tan^{-1}\left(\frac{-Y}{Z-H/2}\right) & Z > -H/2 \end{cases};$$

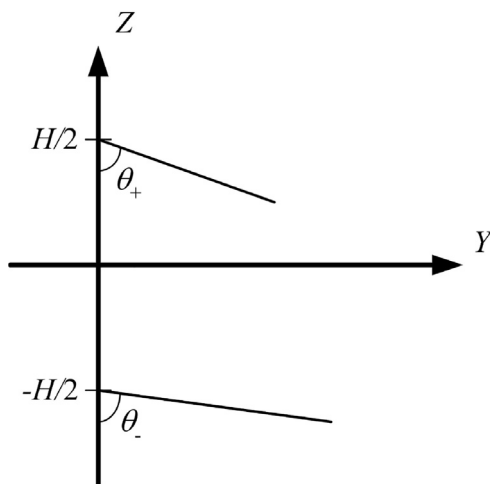


Fig. A.1. Schematic showing how θ_- and θ_+ are defined.

thus, the idea is now to reformulate the problem in terms of $\tilde{\mathcal{B}}_Y$ as the dependent variable, rather than \mathcal{B}_Y . Thus, since θ_- and θ_+ are both harmonic, they make no contribution to the right-hand side of Eqs. (83), and Eqs. (83)–(87) would now become, for $i = a, s$,

$$(2\pi\Omega_i + \Delta^2) \left\{ \tilde{\mathcal{B}}_Y + \beta_- \left(1 - \frac{\theta_-}{\pi} \right) - \beta_+ \left(1 - \frac{\theta_+}{\pi} \right) \right\} = \frac{\partial^2 \tilde{\mathcal{B}}_Y}{\partial Y^2} + \frac{\partial^2 \tilde{\mathcal{B}}_Y}{\partial Z^2}, \tag{A.1}$$

$$(2\pi\Omega_i + \Delta^2) \mathcal{B}_Z = \frac{\partial^2 \mathcal{B}_Z}{\partial Y^2} + \frac{\partial^2 \mathcal{B}_Z}{\partial Z^2}, \tag{A.2}$$

subject to: at $Y = 0$,

$$\frac{\partial \tilde{\mathcal{B}}_Y}{\partial Y} = \begin{cases} i\Delta\bar{\alpha}(Z) - \bar{\beta}'(Z) & \text{for } |Z| \leq H/2 \\ 0 & \text{for } |Z| > H/2 \end{cases}, \tag{A.3}$$

$$\mathcal{B}_Z = \begin{cases} \bar{\beta}(Z) & \text{for } |Z| \leq H/2 \\ 0 & \text{for } |Z| > H/2 \end{cases}; \tag{A.4}$$

as $Y \rightarrow \infty, Z \rightarrow \pm\infty$,

$$\tilde{\mathcal{B}}_Y \sim -\beta_- \left(1 - \frac{\theta_-}{\pi} \right) + \beta_+ \left(1 - \frac{\theta_+}{\pi} \right), \quad \mathcal{B}_Z \rightarrow 0; \tag{A.5}$$

at $Y = 1, |Z| \leq H/2$,

$$\left[\frac{1}{\mu} \left(\frac{\partial \tilde{\mathcal{B}}_Y}{\partial Y} + \frac{1}{\pi} \left(\beta_+ \frac{\partial \theta_+}{\partial Y} - \beta_- \frac{\partial \theta_-}{\partial Y} \right) \right) \right]_-^+ = 0, \tag{A.6}$$

$$[\tilde{\mathcal{B}}_Y]_-^+ = 0, \tag{A.7}$$

$$\left[\frac{\mathcal{B}_Z}{\mu} \right]_-^+ = 0, \tag{A.8}$$

$$\left[\frac{1}{\sigma\mu} \left(\frac{\partial \mathcal{B}_Z}{\partial Y} - \frac{\partial \tilde{\mathcal{B}}_Y}{\partial Z} - \frac{1}{\pi} \left(\beta_+ \frac{\partial \theta_+}{\partial Z} - \beta_- \frac{\partial \theta_-}{\partial Z} \right) \right) \right]_-^+ = 0, \tag{A.9}$$

where

$$\frac{\partial \theta_-}{\partial Y} = \frac{(Z + H/2)}{(Z + H/2)^2 + Y^2}, \quad \frac{\partial \theta_-}{\partial Z} = \frac{Y}{(Z + H/2)^2 + Y^2},$$

$$\frac{\partial \theta_+}{\partial Y} = \frac{(Z - H/2)}{(Z - H/2)^2 + Y^2}, \quad \frac{\partial \theta_+}{\partial Z} = \frac{Y}{(Z - H/2)^2 + Y^2};$$

at $|Z| = H/2, 0 \leq Y \leq 1$,

$$\left[\frac{1}{\mu} \frac{\partial \mathcal{B}_Z}{\partial Z} \right]_-^+ = 0, \tag{A.10}$$

$$\left[\frac{1}{\mu} \left(\tilde{\mathcal{B}}_Y + \beta_- \left(1 - \frac{\theta_-}{\pi} \right) - \beta_+ \left(1 - \frac{\theta_+}{\pi} \right) \right) \right]_{-}^{+} = 0, \quad (\text{A.11})$$

$$[\mathcal{B}_Z]_{-}^{+} = 0, \quad (\text{A.12})$$

$$\left[\frac{1}{\sigma \mu} \left(\frac{\partial \mathcal{B}_Z}{\partial Y} - \frac{\partial \tilde{\mathcal{B}}_Y}{\partial Z} - \frac{1}{\pi} \left(\beta_+ \frac{\partial \theta_+}{\partial Z} - \beta_- \frac{\partial \theta_-}{\partial Z} \right) \right) \right]_{-}^{+} = 0. \quad (\text{A.13})$$

Thus, although the algebra has now become more cumbersome, the equations are at least free of singularities at $Y = 0$, $|Z| = H/2$.

References

- [1] A.A. Tzavaras, H.D. Brody, Electromagnetic stirring and continuous-casting - achievements, problems, and goals, *J. Metals* 36 (1984) 31–37.
- [2] S.-M. Cho, B.G. Thomas, Electromagnetic forces in continuous casting of steel slabs, *Metals* 7 (2019) Article number 471 (38 pages).
- [3] M. Dubke, K.-H. Tacke, K.-H. Spitzer, K. Schwerdtfeger, Flow fields in electromagnetic stirring of rectangular strands with linear inductors: Part I. Theory and experiments with cold models, *Metall. Mater. Trans. B* 19B (1988) 581–593.
- [4] M. Dubke, K.-H. Tacke, K.-H. Spitzer, K. Schwerdtfeger, Flow fields in electromagnetic stirring of rectangular strands with linear inductors: Part II. Computation of flow fields in billets, blooms, and slabs of steel, *Metall. Mater. Trans. B* 19B (1988) 595–602.
- [5] M. Dubke, K.H. Spitzer, K. Schwerdtfeger, Spatial-distribution of magnetic-field of linear inductors used for electromagnetic stirring in continuous-casting of steel, *Ironmak. Steelmak.* 18 (1991) 347–353.
- [6] A.S. Nick, M. Vynnycky, On longitudinal electromagnetic stirring in the continuous casting of steel blooms, *J. Engrg. Math.* 120 (2020) 129–151.
- [7] A.S. Nick, M. Vynnycky, P.G. Jönsson, Analysis of a model for longitudinal electromagnetic stirring in the continuous casting of steel, *Int. J. Appl. Electromag. Mech.* 66 (2021) 35–61.
- [8] M. Vynnycky, On an anomaly in the modeling of electromagnetic stirring in continuous casting, *Metall. Mater. Trans. B* 49B (2018) 399–410.
- [9] P. Monk, *Finite Element Methods for Maxwell's Equations*, Oxford University Press, 2003.
- [10] *Engineering ToolBox, Permeability*, 2016, [online] Available at: Accessed152022.
- [11] A. Zebib, G.M. Homsy, E. Meiburg, High Marangoni number convection in a square cavity, *Phys. Fluids* 28 (1985) 3467–3476.
- [12] B.M. Carpenter, G.M. Homsy, High Marangoni number convection in a square cavity. 2, *Phys. Fluids A* 2 (1990) 137–149.
- [13] X. Wang, Y. Fautrelle, J. Etay, R. Moreau, A periodically reversed flow driven by a modulated traveling magnetic field: Part I. Experiments with GaInSn, *Metall. Mater. Trans. B* 40 (2009) 82–90.
- [14] S. Eckert, P.A. Nikrityuk, D. Raebiger, K. Eckert, G. Gerbeth, Efficient melt stirring using pulse sequences of a rotating magnetic field: Part I. Flow field in a liquid metal column, *Metall. Mater. Trans. B* 38 (2007) 977–988.
- [15] L.S. Beitelman, C.P. Curran, J.D. Lavers, G. Tallback, Modulated electromagnetic stirring of metals at advanced stage of solidification, *EP Patent App.* EP20, 080, 783, 247 (2011).
- [16] T.T. Natarajan, N. El-Kaddah, Finite element analysis of electromagnetically driven flow in sub-mold stirring of steel billets and slabs, *ISIJ Intl.* 38 (1998) 680–689.
- [17] J.T. Huang, E.G. Wang, J.C. He, Numerical simulation of linear electromagnetic stirring in secondary cooling region of slab caster, *J. Iron Steel Res. Intl.* 10 (2003) 16–21.